ACS APPLIED MATERIALS & INTERFACES

Research Article

www.acsami.org

Amplified and Localized Photoswitching of TiO_2 by Micro- and Nanostructuring

Sasha Hoshian,*[,†] Ville Jokinen,[†] Klas Hjort,[‡] Robin H. A. Ras,[§] and Sami Franssila*[,†]

[†]School of Chemical Technology, Department of Materials Science and Engineering, [§]School of Science, Department of Applied Physics, Aalto University, FI-02150 Espoo, Finland

[‡]Division of Microsystems Technology, Uppsala University, SE-752 37 Uppsala, Sweden

Supporting Information

ABSTRACT: Fast photoswitching of wetting properties is important for the development of micro/nanofluidic systems and lab-on-a-chip devices. Here, we show how structuring the surface amplifies photoswitching properties. Atomic layer-deposited titanium dioxide (TiO_2) has phototunable hydrophilic properties due to its surface chemistry, but microscale overhang pillars and additional nanoscale topography can override the chemistry and make the surface superhydrophobic. Three switching processes are achieved simply by controlling the UV exposure time: from (1) rolling superhydrophobic to sticky superhydrophobic (Cassie–Baxter to Wenzel), (2) superhydrophobic to hydrophilic, and (3) superhydrophobic to superhydrophilic after 1, 5, and 10 min of UV exposure, respectively. We report the fastest reversible switching to date: 1 min of UV exposure is enough to promote a rolling-to-sticky transition, and mild heating (30 min at 60 °C) is sufficient for recovery. This performance is caused by a combination of the photoswitching properties of TiO_2, the micropillar overhang geometry, and surface nanostructuring. We demonstrate that the switching also can be performed locally by introducing microwriting under a water droplet.

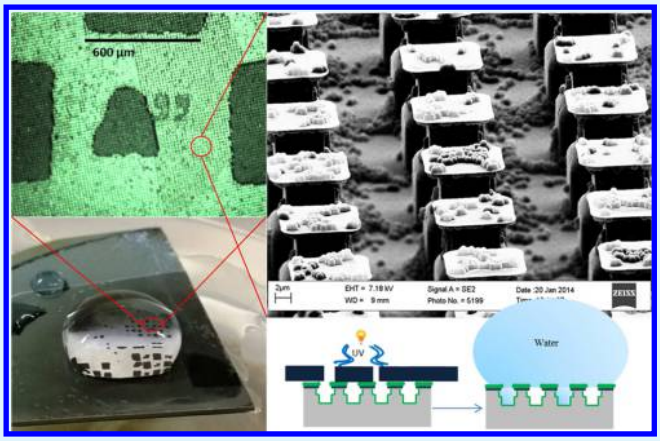

KEYWORDS: *superhydrophobic, overhang structures, wetting transition, microwriting, atomic layer deposition*

1. INTRODUCTION

Controlling the wettability of surfaces may solve a range of practical problems in a variety of applications such as biosensing,[1−4] self-cleaning,[5−7] solar cells,[8] microfluidic devices,[9−12] droplet splitting,[13] directional wetting,[14] and liquid−liquid extraction.[15] The key to such control is to find binary states with different wetting properties. There are two superhydrophobic states: a rolling state with low hysteresis (Cassie−Baxter (CB) state) and a sticky state with high hysteresis (Wenzel (W) state). The important point is the contact angle hysteresis θ_H, which is the difference between the advancing and receding contact angles: a small θ_H (0−15°) equals a rolling state and a larger θ_H equals a sticky state.[16]

Recently, the manipulation of wettability and adhesion on superhydrophobic surfaces has been reported using different approaches such as in situ surface modification using inkjet printing,[16,17] photoelectric polymers,[18] and femtosecond laser irradiation.[19] The photoresponsive wettability of inorganic oxides (e.g., titanium dioxide, zinc oxide, and tungsten oxide) originates from a transition between bistable states of the materials.[3,6,20−34] TiO_2 is an interesting material due to its attractive physicochemical properties that makes it important in optical, photochemical, catalytic, and sensor applications. The water contact angle (WCA) of flat and smooth atomic layer-deposited (ALD) TiO_2 surfaces ranges from 35° to 70°, depending on the thickness and deposition temperature, and it is reduced to 5° by exposing the surface to UV light for hours.[35] After long periods of storage in the dark, the surface reverts to its original state. Upon UV exposure, excess holes diffuse to the

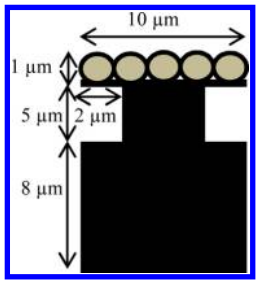

Figure 1. Schematic of a hierarchical overhang structure along with its dimensions.

Received: May 18, 2015
Accepted: June 26, 2015
Published: June 26, 2015

ACS Publications © 2015 American Chemical Society

DOI: 10.1021/acsami.5b04309
ACS Appl. Mater. Interfaces 2015, 7, 15593−15599

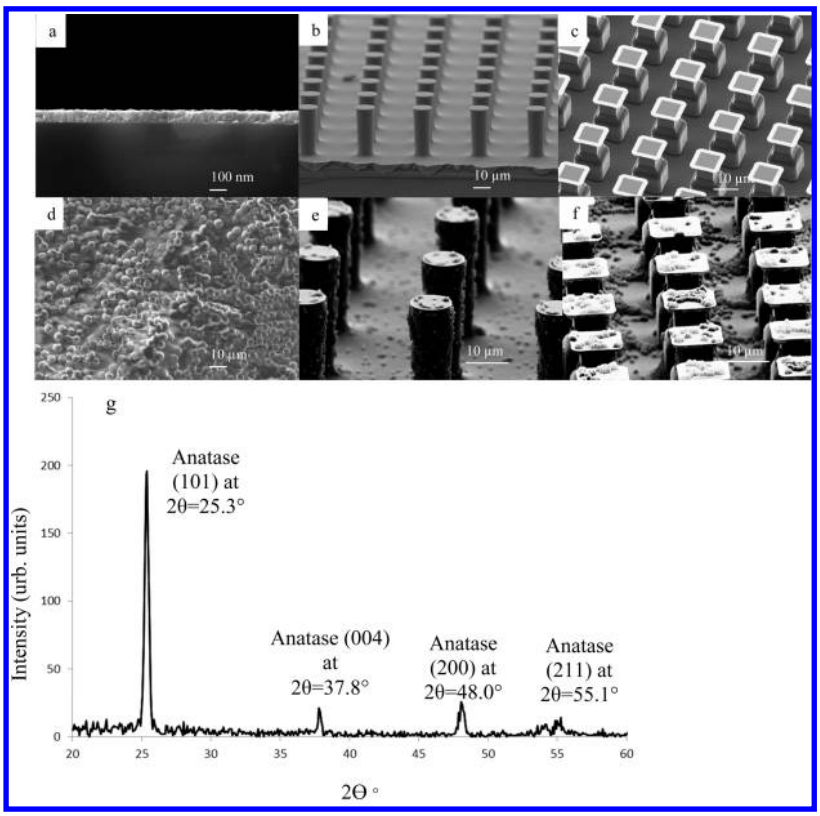

Figure 2. SEM micrographs of the six types of samples studied herein. All samples have 100 nm ALD TiO_2 coating on them: (a) flat substrate, (b) simple micropillars, (c) micropillars with overhang, (d) flat nanostructured surface, (e) simple micropillar with nanostructures, and (f) micro/nanostructured overhangs. (g) XRD measurement of ALD TiO_2.

TiO_2 surface and are trapped on oxygen sites of the lattice. Consequently, the bonds between titanium and lattice oxygen become weak due to the trapped holes. The bonds can be broken and react with water molecules to form new hydroxyl groups, which increase the surface's hydrophilicity.[32]

Because superhydrophobicity of inherently hydrophilic oxides is not straightforward, there are not many reports on the topic, and there are even fewer on photoswitching.

Superhydrophobic ALD TiO_2 without a hydrophobic coating has been reported once before, by coating a lotus leaf with ALD TiO_2, but 2 h of UV exposure reduced the WCA only from 153° to 151°, which is not considered to be photoswitching.[36] It should be noted that there are many papers reporting switchable superhydrophobic TiO_2 surfaces using hydrophobic coatings.[37−39] However, these depend on the decomposition of the hydrophobic coating upon UV exposure, which is time-consuming and, most often, irreversible.

Conventional methods to deposit TiO_2, such as hydrothermal deposition or nanoparticle sintering, are time-consuming, and the resulting films are not mechanically robust. ALD is an ideal technique for nanocoating because of its excellent layer thickness control and conformality.[40] ALD is based on self-limiting irreversible surface reactions: precursor atoms chemisorb onto the surface at (sub)monolayer coverage, and the excess is removed by purging with an inert gas. The second precursor is selected to form covalent bonds with the first. By exposing the substrate at low pressure (1−10 mbar) and suitable temperature (150−500 °C) to cyclic pulses of precursors, a solid thin film is deposited (even though, in practice, the layer thickness per cycle is less than one atomic layer). Alternating pulses of metal- and oxygen-containing precursors lead to metal oxide deposition.[41−43] ALD oxides usually have a hydrophilic nature due to the last step of the process, which leaves the surface terminated with hydroxyl groups.[44,45]

Another important factor that affects wettability is the structuring of the surface. On the basis of the Cassie−Baxter model, the hydrophobicity of a rough surface is due to micro/nanometer scale air pockets trapped under the liquid droplet, leading to a composite interface.[46,47] The Cassie−Baxter equation is written as

$$\cos\theta_{CB} = -1 + \varphi_S(1 + \cos\theta) \quad (1)$$

where θ is the Young contact angle, θ_{CB} refers to the apparent contact angle on the textured surface, and Φ_S is the fraction of the solid in contact with the liquid. On the basis of the Cassie−Baxter model and overhanging (re-entrant) surface geometries, there are some cases where structures can dominate over the chemistry.[47] This means that, no matter what the native contact angle of the smooth surface is, specific structuring can make the surface superhydrophobic.

We show an enhancement of three types of photo/thermal switching: (1) reversible rolling-to-sticky superhydrophobic states, (2) reversible superhydrophobic to hydrophilic states, and (3) reversible superhydrophobic to superhydrophilic states. The first demands control of the hysteresis while the two others depend on the control of the contact angle.

2. RESULTS AND DISCUSSION

2.1. Water Contact Angle Measurements. We have tailored surface wettability by generating structures having multiscale roughness with an overhang. Key dimensions of our test structures are shown in Figure 1. The micro/nano structures

DOI: 10.1021/acsami.5b04309
ACS Appl. Mater. Interfaces 2015, 7, 15593−15599

Table 1. Water Contact Angle Measurements of TiO_2-Coated Test Structures

Static water contact angle	a) flat	b) simple micropillars	c) overhang micropillars	d) flat nanostructured	e) simple micropillars with nanostructure	f) micro-nanostructured overhang pillars
Schematic						
Before UV exposure	35±1°	102±1°	132±1°	67±2°	130±1°	161±1° (Hysteresis 2°)
After 1 min UV exposure	30±1°	98±1°	122±1°	62±1°	124±1°	150±1° (Hysteresis 100°)
Recovery to original state in oven at 60°C	3 days	3 days	30 minutes	3 days	3 days	30 minutes
After 5 min UV exposure	27±1°	92±1°	43±1°	58±1°	120±1°	51±1°
Recovery to original state in oven at 60°C	1 week	1 week	1 hour	1 week	1 week	1 hour
After 10 min UV exposure	25±1°	75±1°	0°	54±1°	100±1°	0°
Recovery to original state in oven at 60°C	2 weeks	2 weeks	2 hours	2 weeks	2 weeks	2 hours
After 15 min UV exposure	10±1°	37±1°	0°	50±2°	45±1°	0°
Recovery to original state in oven at 60°C	3 weeks	3 weeks	2 hours	3 weeks	3 weeks	2 hours
After 20 min UV exposure	0°	24±1°	0°	0°	0°	0°
Recovery to original state in oven at 60°C	4 weeks	4 weeks	2 hours	4 weeks	4 weeks	2 hours

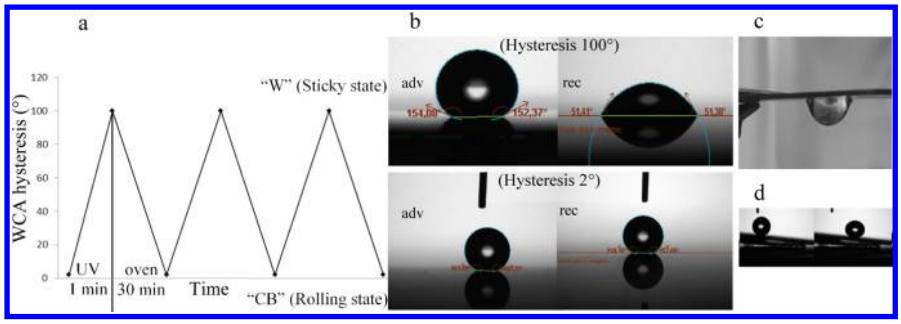

Figure 3. Rolling-to-sticky transitions of nanostructured overhang pillars by repeated UV exposure and oven recovery: (a) water contact angle hysteresis transition between Cassie and Wenzel states. (b) Before UV exposure, hysteresis is 2°; after exposure, it is 100°. (c) A droplet sticks to the sample after UV exposure. (d) Sliding angle of 5° for the sample before UV exposure.

amplify small changes in the TiO_2 surface chemistry upon UV exposure, and, similarly, the recovery of the surface by heating is much faster. The fabrication process and characterization of the micro- and nanostructure's parameters are explained in the Supporting Information (Figures S1−S5).

We studied the wetting switchability of six different types of samples: (1) flat substrate (Figure 2a), (2) simple micropillars without nanostructures (Figure 2b), (3) overhang structures without nanostructures (Figure 2c), (4) flat nanostructured surface (Figure 2d), (5) simple micropillars with nanostructuring (Figure 2e), and (6) micro/nanostructured overhang structures (Figure 2f). All surfaces are covered by a 100 nm thick ALD TiO_2 layer. Figure 2g displays the X-ray diffraction (XRD) patterns of 100 nm ALD TiO_2 (5 nm deposited at 70 °C followed by 95 nm deposited at 300 °C). A (101) peak at 25.3°, (004) at 37.8°, (200) at 48°, and (211) at 55.1° are attributed to anatase phase.[48] JCPDS card number 190 was used to identify the crystalline anatase phase.

DOI: 10.1021/acsami.5b04309
ACS Appl. Mater. Interfaces 2015, 7, 15593−15599

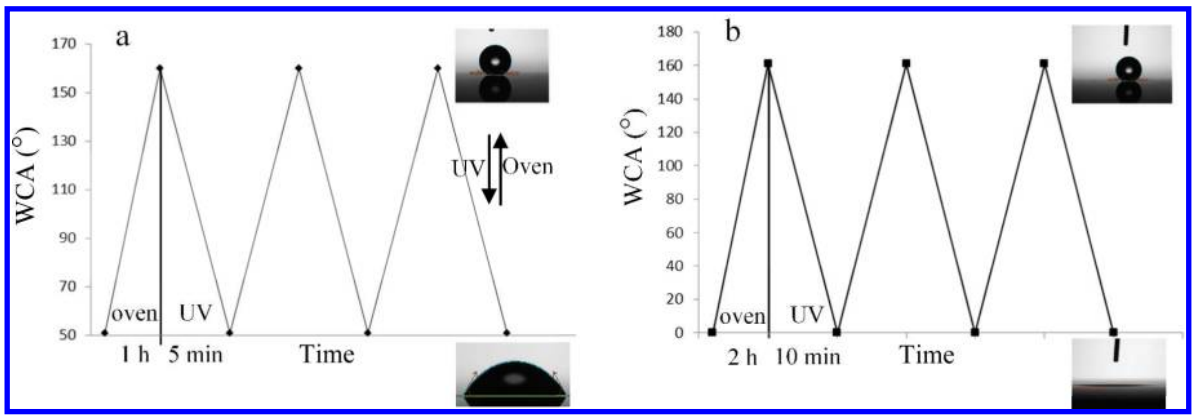

Figure 4. (a) Hydrophilic to superhydrophobic transitions by 1 h annealing in oven at 60 °C and 5 min of UV exposure; (b) superhydrophilic to superhydrophobic transitions by 2 h annealing in oven at 60 °C and 10 min of UV exposure.

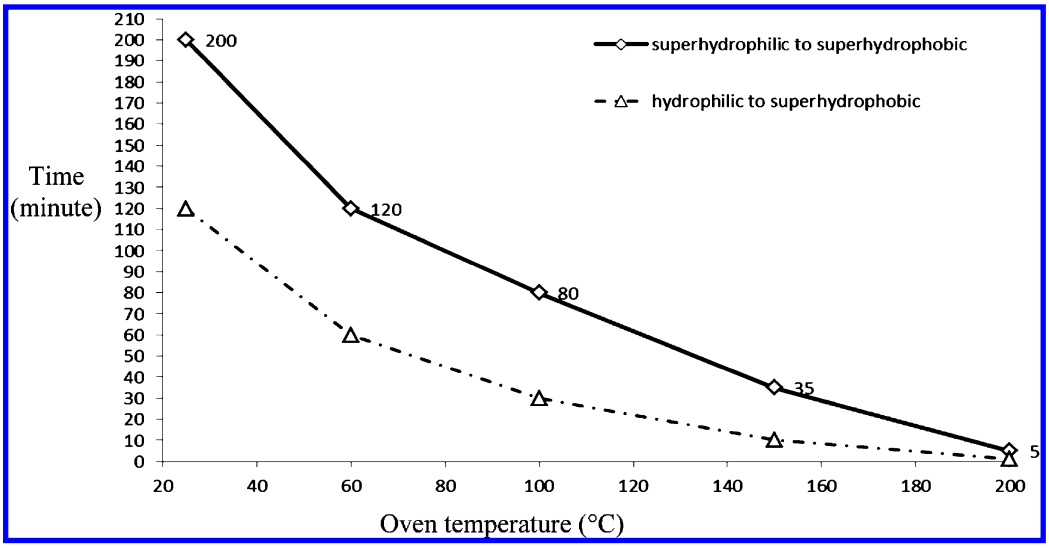

Figure 5. Recovery time as a function of temperature for nanostructured overhang pillars.

Schematics of the samples as well as water contact angles and recovery times are presented in Table 1.

Water contact angles before UV exposure ranged from 35° to 161° for samples 1−6. The micro/nanostructured overhang pillars were superhydrophobic (Movie S1), with a small sliding angle of 5°, even though the flat surface was hydrophilic. Nanostructuring increased the WCA, but it did not improve the photoswitching, whereas microscale overhang structures did. One minute of UV exposure reduced the WCA by 10° and 11° for overhang pillars (Figure 2c,f), but it caused only 4° and 6° reductions for simple micropillars (Figure 2b,e). It is important to note that nanostructuring plays a critical role in the WCA; without it, superhydrophobicity is not achieved.

2.2. Reversible Rolling-to-Sticky Switching. UV exposure at 365 nm for as little as 1 min (20 mW/cm^2 corresponding to 1200 mJ/cm^2) is enough to switch the micro/nanostructured overhang pillars from a rolling to a sticky state. The contact angle change was only 11° (from 161° to 150°), but the contact angle hysteresis went from 2° to 100°.

A 1 min transition is fast compared to reports in the literature:[28,30,49] in ref 28, it was 20 min, in ref 30, it was 100 min, and in ref 49, it was 180 min. Increasing the UV exposure time further reduced WCAs on all structures, but this effect was more dramatic on samples with micro/nanostructured overhang pillars. UV exposure for 10 min renders the micro/nanostructured overhang pillars superhydrophilic.

Overhang structures improve the recovery of the samples to their original wetting states. The micro/nanostructured overhang samples exposed to UV for 1 min recovered to a superhydrophobic Cassie−Baxter state in 30 min at 60 °C. Figure 3 shows three cycles of rolling-to-sticky reversible transitions. Recovery time to the original wetting state is at least 100 times faster than that for samples without overhang structures (Table 1).

2.3. Reversible Superhydrophobic to Hydrophilic. The second type of switching transition, from superhydrophobic (WCA 160°) to hydrophilic (WCA 51°), using micro/nanostructured overhang pillars was achieved by 5 min of UV exposure (Movie S2), and the process was reversible: 1 h annealing at 60 °C recovered the 160° WCA (Figure 4a). The flat reference sample actually became more hydrophilic (WCA 27°), but its recovery took 1 week in oven at 60 °C.

2.4. Reversible Superhydrophobic to Superhydrophilic. The third type of switching, from superhydrophobic (161°) to superhydrophilic (0°), was achieved by exposing the micro/nanostructured overhang pillars to UV for 10 min (Movie S3). Fully reversible recovery took 2 h at 60 °C (Figure 4b). Increasing the oven temperature reduced the superhydrophilic to superhydrophobic recovery time to as few as 5 min when 200 °C was utilized, as shown in Figure 5.

DOI: 10.1021/acsami.5b04309
ACS Appl. Mater. Interfaces 2015, 7, 15593−15599

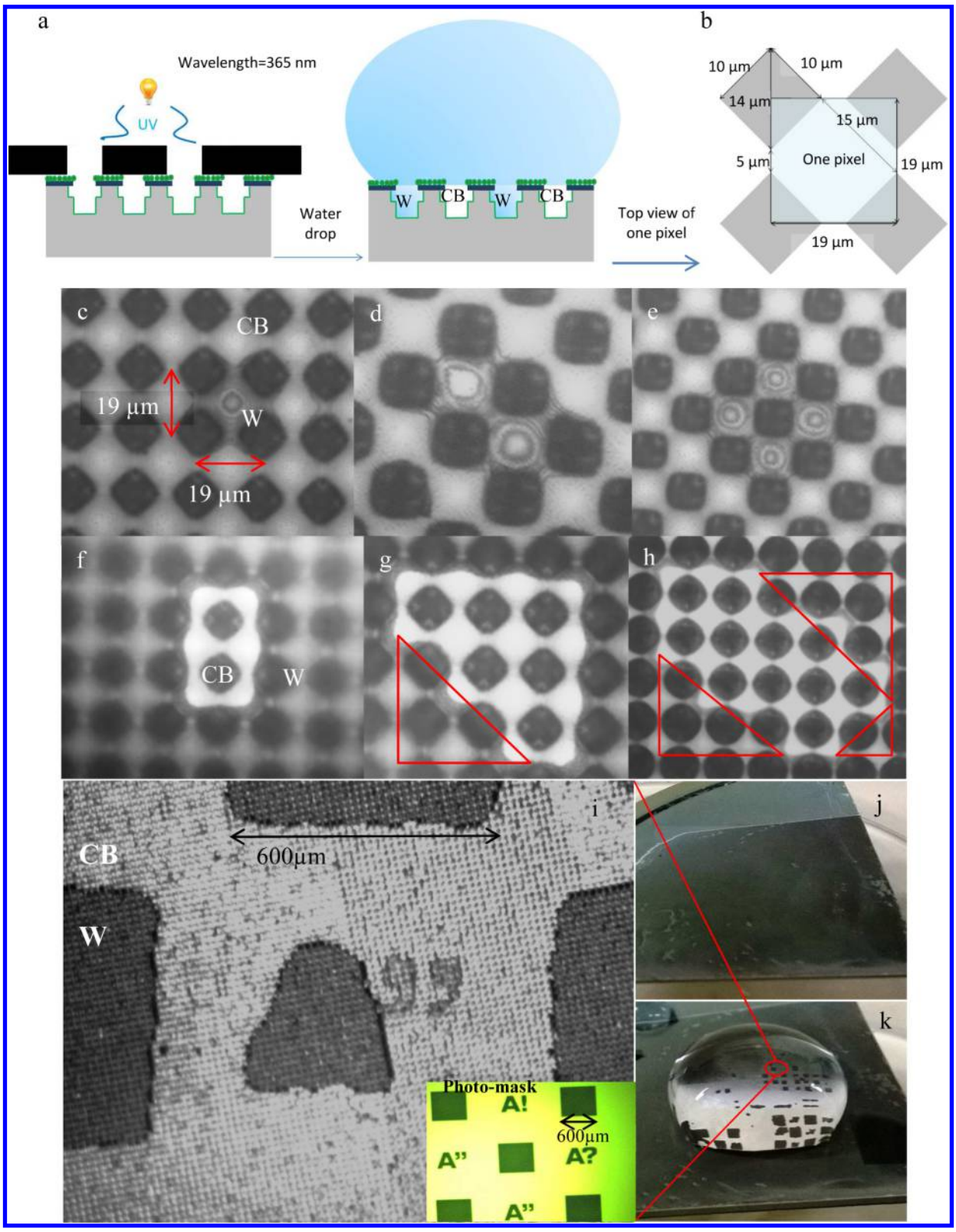

Figure 6. Microwriting under a water droplet. (a) Masked UV exposure of TiO_2-coated micro/nanostructured overhang pillars. The water droplet penetrates between the pillars in the exposed areas (W state) and displays contrast with the CB state. (b) Top-view schematic of one pixel with a size of 361 μm^2. Microscopy images show the resolution of the microwriting under a water droplet. Dots have sizes down to (c) 361 μm^2, (d) 2×361 μm^2, and (e) 4×361 μm^2 in area; holes have sizes down to (f) 2×361 μm^2, (g) 9×361 μm^2, and (h) 20×361 μm^2 in area (pillars are 10×10 μm^2). (i) Optical microscope image of the Aalto University logo under a water droplet. Micro/nanostructured overhang pillars after 1 min of UV exposure through a photomask: (j) without a water droplet, the pattern is invisible; (k) with a water droplet, the pattern becomes visible.

A theoretical mechanism for photo/thermal switching of these surfaces involves the formation and removal of hydroxyl groups. Upon UV exposure, the bonds between titanium and lattice oxygen become weak due to the trapped holes and can be broken

DOI: 10.1021/acsami.5b04309
ACS Appl. Mater. Interfaces 2015, 7, 15593−15599

and react with water molecules to form new hydroxyl groups, which increase the surface's hydrophilicity.[32] On the other hand, annealing speeds the replacement of absorbed hydroxyl groups with atmospheric oxygen and the TiO_2 becomes less hydrophilic.[32] After enough annealing time has occurred, water cannot penetrate between the pillars, and microair pockets remain there. According to the Cassie equation, the apparent contact angle becomes greater than 90° and the surface becomes superhydrophobic, back to its original state. The amount of hydroxyl groups formed/removed can be tuned through the exposure/annealing time. This process is amplified in the structure introduced here due to more air pockets being trapped below the T-shaped micropillars.

2.5. Microwriting under a Water Droplet. Locally engineering the wetting properties of surfaces has been reported using external stimuli such as pressure,[11] electrochemistry,[50] and acoustic waves.[51] We also demonstrate microwriting under a water droplet by performing a localized CB-to-W transition. Photomasked UV exposure was carried out (Figure 6a) to produce a contrast in the surface energy on the TiO_2-coated micronanostructured overhang pillars. Water penetrated between pillars that were exposed to UV locally, whereas the rest of the droplet remained on top of the pillars in a CB state. The contrast is invisible at the solid−air interface, but it became visible under the water droplet. The resolution of the writing (size of a unit pixel) was defined by the size and spacing of the pillars, 10 and 5 μm, respectively. A schematic of one pixel with its dimensions is shown in Figure 6b. Optical microscopy images of a 1 min UV-exposed sample show dots (W surrounded by CB; Figure 6c−e) and holes (CB surrounded by W; Figure 6f−h). The latter is more demanding because of the instability of water on CB when it is surrounded by W states due to the concave shape of the meniscus.[52] The red triangles in Figure 6g−h show wetting defects due to a CB-to-W transition during imaging under the microscope. Figure 6i−k shows a sample exposed through a photomask with an Aalto University logo.

3. CONCLUSIONS

We have shown a new approach that can significantly increase the speed of wetting transitions. Three types of fast photo/thermal switching processes were demonstrated: from (1) rolling to sticky superhydrophobic states, (2) superhydrophobic to hydrophilic states, and (3) superhydrophobic to superhydrophilic states. The key elements for this process are a photoactive TiO_2 thin film, the overhang geometry of the micropillars, and nanoscale surface structuring.

The switching speeds are still too slow for practical applications, even though the water droplets do not significantly evaporate during 1 min of UV exposure and annealing at low temperature. Nonaqueous solutions with higher boiling points should be favorable in this respect.

Locally programming the surface energy of the hierarchical overhang structured surface was achieved by photomasked UV exposure, resulting in microwriting under a water droplet. Optical contrast between Cassie−Baxter and Wenzel states makes the pattern visible under the water droplet. By decreasing the pillar dimensions and pitches, we expect to improve the pixel density 100-fold. Programming might be very useful for local material deposition from solutions[53,54] for biosensing.[55]

■ ASSOCIATED CONTENT

Supporting Information

Fabrication process (Figure S1), characterization of micro- and nanostructure parameters (Figures S2−S6 and Table S1), and movies (S1−S3) showing a water droplet on a hierarchical overhang sample before and after UV exposure. The Supporting Information is available free of charge on the ACS Publications website at DOI: 10.1021/acsami.5b04309.

■ AUTHOR INFORMATION

Corresponding Authors

*(S.H.) E-mail: sasha.hoshian@aalto.fi.
*(S.F.) E-mail: sami.franssila@aalto.fi.

Notes

The authors declare no competing financial interest.

■ ACKNOWLEDGMENTS

This research was supported by the Academy of Finland (PROWET project nos. 263538, 263560, and 266820). Wafer processing took place at the Aalto Nanofab cleanroom. The authors acknowledge Sakari Sintonen for his help with XRD measurements.

■ REFERENCES

(1) Kim, J.-Y.; Choi, K.; Moon, D.-I.; Ahn, J.-H.; Park, T. J.; Lee, S. Y.; Choi, Y.-K. Surface Engineering for Enhancement of Sensitivity in an Underlap-FET Biosensor by Control of Wettability. *Biosens. Bioelectron.* **2013**, *41*, 867−870.

(2) Kim, J.; Park, H.; Kang, B.; Ku, R.; Ham, C.; Yang, M. Highly Effective Gold Nanoparticle-Enhanced Biosensor Array on the Wettability Controlled Substrate by Wiping. *J. Appl. Phys.* **2011**, *110*, 084701.

(3) Zhang, Z.; Chen, H.; Zhong, J.; Saraf, G.; Lu, Y. Fast and Reversible Wettability Transitions on ZnO Nanostructures. *J. Electron. Mater.* **2007**, *36*, 895−899.

(4) Jokinen, V.; Sakha, P.; Suvanto, P.; Rivera, C.; Franssila, S.; Lauri, S. E.; Huttunen, H. J. A Microfluidic Chip for Axonal Isolation and Electrophysiological Measurements. *J. Neurosci. Methods* **2013**, *212* (2), 276−282.

(5) Anastasiadis, S. H. Development of Functional Polymer Surfaces with Controlled Wettability. *Langmuir* **2013**, *29*, 9277−9290.

(6) Laurenti, M.; Cauda, V.; Gazia, R.; Fontana, M.; Rivera, V. F.; Bianco, S.; Canavese, G. Wettability Control on ZnO Nanowires Driven by Seed Layer Properties. *Eur. J. Inorg. Chem.* **2013**, *2013*, 2520−2527.

(7) Yao, X.; Song, Y.; Jiang, L. Applications of Bio-Inspired Special Wettable Surfaces. *Adv. Mater.* **2011**, *23*, 719−734.

(8) Sainiemi, L.; Jokinen, V.; Shah, A.; Shpak, M.; Aura, S.; Suvanto, P.; Franssila, S. Non-Reflecting Silicon and Polymer Surfaces by Plasma Etching and Replication. *Adv. Mater.* **2011**, *23* (1), 122−126.

(9) Schneider, M. H.; Willaime, H.; Tran, Y.; Rezgui, F.; Tabeling, P. Wettability Patterning by UV-Initiated Graft Polymerization of Poly(acrylic acid) in Closed Microfluidic Systems of Complex Geometry. *Anal. Chem.* **2010**, *82*, 8848−8855.

(10) Almutairi, Z.; Ren, C. L.; Simon, L. Evaluation of Polydimethylsiloxane (PDMS) Surface Modification Approaches for Microfluidic Applications. *Colloids Surf., A* **2012**, *415*, 406−412.

(11) Verho, T.; Korhonen, J. T.; Sainiemi, L.; Jokinen, V.; Bower, C.; Franze, K.; Franssila, S.; Andrew, P.; Ikkala, O.; Ras, R. H. A. Reversible Switching Between Superhydrophobic States on a Hierarchically Structured Surface. *Proc. Natl. Acad. Sci. U. S. A.* **2012**, *109* (26), 10210−10213.

(12) Jokinen, V.; Franssila, S. Capillarity in Microfluidic Channels with Hydrophilic and Hydrophobic Walls. *Microfluid. Nanofluid.* **2008**, *5* (4), 443−448.

(13) Jokinen, V.; Sainiemi, L.; Franssila, S. Complex Droplets on Chemically Modified Silicon Nanograss. *Adv. Mater.* **2008**, *20* (18), 3453−3456.

(14) Jokinen, V.; Leinikka, M.; Franssila, S. Microstructured Surfaces for Directional Wetting. *Adv. Mater.* **2009**, *21* (47), 4835−4838.

(15) Jokinen, V.; Kostiainen, R.; Sikanen, T. Multiphase Designer Droplets for Liquid-Liquid Extraction. *Adv. Mater.* **2012**, *24* (46), 6240−6243.

DOI: 10.1021/acsami.5b04309
ACS Appl. Mater. Interfaces 2015, 7, 15593−15599

(16) Lai, Y.; Pan, F.; Xu, C.; Fuchs, H.; Chi, L. In Situ Surface-Modification-Induced Superhydrophobic Patterns with Reversible Wettability and Adhesion. *Adv. Mater.* **2013**, *25*, 1682−1686.
(17) Huang, J. Y.; Lai, Y. K.; Pan, F.; Yang, L.; Wang, H.; Zhang, K. Q.; Fuchs, H.; Chi, L. F. Multifunctional Superamphiphobic TiO2 Nanostructure Surfaces with Facile Wettability and Adhesion Engineering. *Small* **2014**, *10* (23), 4865−4873.
(18) Xu, L.; Lu, X.; Li, M.; Lu, Q. Reversible Switching of Water-Droplet Adhesion on a Superhydrophobic Polythiophene Surface. *Adv. Mater. Interfaces* **2014**, *1*, 1400011.
(19) Long, J.; Fan, P.; Gong, D.; Jiang, D.; Zhang, H.; Li, L.; Zhong, M. Superhydrophobic Surfaces Fabricated by Femtosecond Laser with Tunable Water Adhesion: From Lotus Leaf to Rose Petal. *ACS Appl. Mater. Interfaces* **2015**, *7*, 9858−9865.
(20) Caputo, G.; Nobile, C.; Kipp, T.; Blasi, L.; Grillo, V.; Carlino, E.; Manna, L.; Cingolani, R.; Cozzoli, P. D.; Athanassiou, A. Reversible Wettability Changes in Colloidal TiO2 Nanorod Thin-Film Coatings under Selective UV Laser Irradiation. *J. Phys. Chem. C* **2008**, *112*, 701−714.
(21) Lai, Y.; Gao, X.; Zhuang, H.; Huang, J.; Lin, C.; Jiang, L. Designing Superhydrophobic Porous Nanostructures with Tunable Water Adhesion. *Adv. Mater.* **2009**, *21*, 3799−3803.
(22) Lai, Y.; Lin, C.; Huang, J.; Zhuang, H.; Sun, L.; Nguyen, T. Markedly Controllable Adhesion of Superhydrophobic Spongelike Nanostructure TiO2 Films. *Langmuir* **2008**, *24*, 3867−3873.
(23) Liu, X.; Cai, M.; Liang, Y.; Zhou, F.; Liu, W. Photo-Regulated Stick-Slip Switch of Water Droplet Mobility. *Soft Matter* **2011**, *7*, 3331−3336.
(24) Malm, J.; Sahramo, E.; Karppinen, M.; Ras, R. H. A. Photo-Controlled Wettability Switching by Conformal Coating of Nanoscale Topographies with Ultrathin Oxide Films. *Chem. Mater.* **2010**, *22*, 3349−3352.
(25) Sawunyama, P.; Yasumori, A.; Okada, K. The Nature of Multilayered TiO2-Based Photocatalytic Films Prepared By a Sol-Gel Process. *Mater. Res. Bull.* **1998**, *33*, 795−801.
(26) Wang, S.; Song, Y.; Jiang, L. Photoresponsive Surfaces with Controllable Wettability. *J. Photochem. Photobiol., C* **2007**, *8*, 18−29.
(27) Xin, B.; Hao, J. Reversibly Switchable Wettability. *Chem. Soc. Rev.* **2010**, *39*, 769−782.
(28) Xu, Q. F.; Liu, Y.; Lin, F.-J.; Mondal, B.; Lyons, A. M. Superhydrophobic TiO2−Polymer Nanocomposite Surface with UV-Induced Reversible Wettability and Self-Cleaning Properties. *ACS Appl. Mater. Interfaces* **2013**, *5*, 8915−8924.
(29) Yu, J.; Zhao, X.; Zhao, Q. Effect of Surface Structure on Photocatalytic Activity of TiO2 Thin Films Prepared by Sol-Gel Method. *Thin Solid Films* **2000**, *379*, 7−14.
(30) Zhang, M.; Zhang, T.; Cui, T. Wettability Conversion from Superoleophobic to Superhydrophilic on Titania/Single-Walled Carbon Nanotube Composite Coatings. *Langmuir* **2011**, *27*, 9295−9301.
(31) Zhang, X.; Jin, M.; Liu, Z.; Tryk, D. A.; Nishimoto, S.; Murakami, T.; Fujishima, A. Superhydrophobic TiO2 Surfaces: Preparation, Photocatalytic Wettability Conversion, and Superhydrophobic−Superhydrophilic Patterning. *J. Phys. Chem. C* **2007**, *111*, 14521−14529.
(32) Sakai, N.; Fujishima, A.; Watanabe, T.; Hashimoto, K. Quantitative Evaluation of the Photoinduced Hydrophilic Conversion Properties of TiO2 Thin Film Surfaces by the Reciprocal of Contact Angle. *J. Phys. Chem. B* **2003**, *107* (4), 1028−1035.
(33) Feng, X.; Zhai, J.; Jiang, L. The Fabrication and Switchable Superhydrophobicity of TiO2 Nanorod Films. *Angew. Chem., Int. Ed.* **2005**, *44*, 5115−5118.
(34) Feng, X.; Feng, L.; Jin, M.; Zhai, J.; Jiang, L.; Zhu, D. Reversible Super-hydrophobicity to Super-hydrophilicity Transition of Aligned ZnO Nanorod Films. *J. Am. Chem. Soc.* **2004**, *126*, 62−63.
(35) Huang, Y.; Pandraud, G.; Sarro, P. M. Characterization of Low Temperature Deposited Atomic Layer Deposition TiO2 for MEMS Applications. *J. Vac. Sci. Technol., A* **2013**, *31*, 01A148.
(36) Szilágyi, I. M.; Teucher, G.; Härkönen, E.; Färm, E.; Hatanpää, T.; Nikitin, T.; Khriachtchev, L.; Räsänen, M.; Ritala, M.; Leskelä, M. Programming Nanostructured Soft Biological Surfaces by Atomic Layer Deposition. *Nanotechnology* **2013**, *24*, 245701.
(37) Wang, D.; Liu, Y.; Liu, X.; Zhou, F.; Liu, W.; Xue, Q. Towards a Tunable and Switchable Water Adhesion on a TiO2 Nanotube Film with Patterned Wettability. *Chem. Commun.* **2009**, 7018−7020.
(38) Zhou, S.; Ding, X.; Wu, L. Fabrication of Ambient-Curable Superhydrophobic Fluoropolysiloxane/TiO2 Nanocomposite Coatings with Good Mechanical Properties and Durability. *Prog. Org. Coat.* **2013**, *76*, 563−570.
(39) Kamegawa, T.; Shimizu, Y.; Yamashita, H. Superhydrophobic Surfaces with Photocatalytic Self-Cleaning Properties by Nanocomposite Coating of TiO2 and Polytetrafluoroethylene. *Adv. Mater.* **2012**, *24*, 3697−3700.
(40) George, S. M. Atomic Layer Deposition: An Overview. *Chem. Rev.* **2010**, *110*, 111−131.
(41) Miikkulainen, V.; Leskelä, M.; Ritala, M.; Puurunen, R. L. Crystallinity of Inorganic Films Grown by Atomic Layer Deposition: Overview and General Trends. *J. Appl. Phys.* **2013**, *113*, 021301.
(42) Mitchell, D. R. G.; Triani, G.; Attard, D. J.; Finnie, K. S.; Evans, P. J.; Barbé, C. J.; Bartlett, J. R. Atomic Layer Deposition of TiO2 and Al2O3 Thin Films and Nanolaminates. *Smart Mater. Struct.* **2006**, *15*, S57.
(43) Xie, Q.; Jiang, Y.-L.; Detavernier, C.; Deduytsche, D.; Van Meirhaeghe, R. L.; Ru, G.-P.; Li, B.-Z.; Qu, X.-P. Atomic Layer Deposition of TiO2 From Tetrakis-Dimethyl-Amido Titanium or Ti Isopropoxide Precursors and H2O. *J. Appl. Phys.* **2007**, *102*, 083521.
(44) Alibabaei, L.; Farnum, B. H.; Kalanyan, B.; Brennaman, M. K.; Losego, M. D.; Parsons, G. N.; Meyer, T. J. Atomic Layer Deposition of TiO2 on Mesoporous NanoITO: Conductive Core−Shell Photoanodes for Dye-Sensitized Solar Cells. *Nano Lett.* **2014**, *14*, 3255−3261.
(45) Peng, Q.; Kalanyan, B.; Hoertz, P. G.; Miller, A.; Kim, D. H.; Hanson, K.; Alibabaei, L.; Liu, J.; Meyer, T. J.; Parsons, G. N.; Glass, J. T. Solution-Processed, Antimony-Doped Tin Oxide Colloid Films Enable High-Performance TiO2 Photoanodes for Water Splitting. *Nano Lett.* **2013**, *13*, 1481−1488.
(46) Tuteja, A.; Choi, W.; Ma, M.; Mabry, J. M.; Mazzella, S. A.; Rutledge, G. C.; McKinley, G. H.; Cohen, R. E. Designing Superoleophobic Surfaces. *Science* **2007**, *318*, 1618−1622.
(47) Hoshian, S.; Jokinen, V.; Somerkivi, V.; Lokanathan, A. R.; Franssila, S. Robust Superhydrophobic Silicon without a Low Surface-Energy Hydrophobic Coating. *ACS Appl. Mater. Interfaces* **2015**, *7* (1), 941−949.
(48) Aarik, L.; Arroval, T.; Rammula, R.; Mandar, H.; Sammelselg, V.; Aarik, J. Atomic Layer Deposition of TiO2 from TiCL4 and O3. *Thin Solid Films* **2013**, *542*, 100−107.
(49) Sawai, Y.; Nishimoto, S.; Kameshima, Y.; Fujii, E.; Miyake, M. Photoinduced Underwater Superoleophobicity of TiO2 Thin Films. *Langmuir* **2013**, *29*, 6784−6789.
(50) Zeira, A.; Chowdhury, D.; Maoz, R.; Sagiv, J. Contact Electrochemical Replication of Hydrophilic-Hydrophobic Monolayer Patterns. *ACS Nano* **2008**, *2* (12), 2554−2568.
(51) Dufour, R.; Saad, N.; Carlier, J.; Campistron, P.; Nassar, G.; Toubal, M.; Boukherroub, R.; Senez, V.; Nongaillard, B.; Thomy, V. Acoustic Tracking of Cassie to Wenzel Wetting Transitions. *Langmuir* **2013**, *29* (43), 13129−13134.
(52) Jokinen, V.; Sainiemi, L.; Franssila, S. Controlled Lateral Spreading and Pinning of Oil Droplets Based on Topography and Chemical Patterning. *Langmuir* **2011**, *27* (11), 7314−7320.
(53) Hatton, B. D.; Aizenberg, J. Writing on Superhydrophobic Nanopost Arrays: Topographic Design for Bottom-up Assembly. *Nano Lett.* **2012**, *12*, 4551−4557.
(54) Marín, Á. G.; Gelderblom, H.; Susarrey-Arce, A.; van Houselt, A.; Lefferts, L.; Gardeniers, J. G. E.; Lohse, D.; Snoeijer, J. H. Building Microscopic Soccer Balls with Evaporating Colloidal Fakir Drops. *Proc. Natl. Acad. Sci. U. S. A.* **2012**, *109*, 16455−16458.
(55) Ostuni, E.; Chen, C. S.; Ingber, D. E.; Whitesides, G. M. Selective Deposition of Proteins and Cells in Array of Microwells. *Langmuir* **2001**, *17* (9), 2828−2834.

DOI: 10.1021/acsami.5b04309
ACS Appl. Mater. Interfaces 2015, 7, 15593−15599